www.advenergysustres.com

Constructing a Robust Solid-Electrolyte Interphase Layer via Chemical Prelithiation for High-Performance SiO_x Anode

Shiming Chen, Zijian Wang, Lu Wang, Zhibo Song, Kai Yang, Wenguang Zhao, Lele Liu, Jianjun Fang, Guoyu Qian, Feng Pan,* and Luyi Yang*

Being considered as a promising anode material for next-generation lithium-ion batteries, silicon oxide (SiOx) suffers from low initial coulombic efficiency and unstable solid-electrolyte interphase (SEI), which hinder its commercial use. To address these issues, herein, an optimized chemical prelithiation method is developed using a molecularly engineered lithium-biphenyl-type complex, which facilitates improved prelithiation efficiency. More importantly, owing to the reaction between the prelithiation agent and sodium carboxymethyl cellulose binder, a stable artificial SEI layer with hard inorganic particles embedded in soft organic matrix can be preformed on the surface of the SiOx anode after prelithiation. The preformed SEI layer remains stable during long-term cycling, contributing to significant improvement of capacity retention (87.4%) over pristine SiO_x (68.6%) after 100 cycles at 0.2 C. Through demonstrating a hitherto unknown interfacial constructing strategy for SiOx, this study provides a fresh perspective on realizing high-capacity Si-based anodes.

1. Introduction

Lithium-ion batteries (LIBs) with high energy densities are highly desired for the widespread usage of portable electronic devices and the electric vehicles (EVs). [1-3] Considerable efforts have been devoted to developing high-capacity active materials for next-generation LIBs. [4–7] Recently, silicon oxide (SiO $_x$) has been considered as one of the most promising alternatives to replace commercially used graphite anode owing to its facile synthesis and lower volume swing during cycling (≈118%) compared with elemental Si (≈400%). [8-10] Nevertheless, the

S. Chen, Z. Wang, L. Wang, Z. Song, K. Yang, W. Zhao, L. Liu, J. Fang, G. Qian, F. Pan, L. Yang School of Advanced Materials Peking University Shenzhen Graduate School

Shenzhen 518055, P. R. China

E-mail: panfeng@pkusz.edu.cn; yangly@pkusz.edu.cn

The ORCID identification number(s) for the author(s) of this article can be found under https://doi.org/10.1002/aesr.202200083.

© 2022 The Authors. Advanced Energy and Sustainability Research published by Wiley-VCH GmbH. This is an open access article under the terms of the Creative Commons Attribution License, which permits use, distribution and reproduction in any medium, provided the original work is properly cited.

DOI: 10.1002/aesr.202200083

low initial coulombic efficiency (ICE, \approx 70%) and continuous consumption of electrolyte have limited the extensive commercial application of SiO_{x} . [11,12] Therefore, compensating the Li loss during initial cycles is necessary for successful utilization of SiO_x in high-energy-density full cells.[13,14] Li compensation can be generally divided into two categories: ex situ and in situ methods. Mixing sacrificial additives with active materials is a typical in situ approach, which depends on electrochemical oxidation of additives to compensate the Li loss.^[15,16] However, this method inevitably leads to electrode volume variation and inactive residues in the cell. Ex situ prelithiation includes electrochemical prelithiation and chemical prelithiation. The former method requires disassembling and reassembling of batteries, which

precludes its practical application. [17,18] Alternatively, chemical prelithiation approach is the direct contact between the SiO_x anode and Li-based reducing agents (e.g., Li metal and Li-based organic complex).[19-21] Chemical prelithiation with Li-arene (i.e., aromatic hydrocarbon) complex (LAC) solution has many advantages including homogeneous reaction, controllable reducing potential, and lithiation degree. [22-24]

For efficient chemical lithiation in SiO_x, the electrochemical potentials of arene molecules should be optimized. With their relatively low-lying π^* lowest unoccupied molecular orbital (LUMO), the reducibility of many arenes is suitable for SiO_x. [25] Ideally, the reducing potential of a desirable arene should fall between 0 V versus Li/Li⁺ and the lithiation potential of SiO_x (0.2 V vs Li/Li⁺). If this value is too low, it cannot form a LAC; if this value is too high, the complex cannot chemically lithiate SiO_x anode but rather form a solid-electrolyte interphase (SEI).[19,26] Hence, there is necessary to find a suitable arene structure with sufficient reducing capability to achieve a controllable amount Li content in the SiO_x anode within a reasonable time frame.

Previously, it has been reported that substitution of biphenyls at the para-position can achieve ideal ICE near 100% rather than other positions.^[27] However, the impact of such compounds on SiOx anodes, especially on the SEI, still awaits in-depth investigation. Herein, through theoretically and experimentally screening various electron-donating groups in the para-position

2699412, 2022, 10, Downloaded from https://advanced.onlinelibrary.wiley.com/doi/10.1002/aesr.202200083 by University Town Of Shenzhen, Wiley Online Library on [24/11/2025]. See the Term

on Wiley Online Library for rules of use; OA articles are governed by the applicable Creative Commons I

of biphenyl to adjust its reduction potential, we proposed an LAC 4,4'-diethyl biphenyl (DEBP) with an ideal redox potential which enables more efficient prelithiation. More importantly, owing to the presence of sodium carboxymethyl cellulose (CMC-Na) binder, a stable SEI can be formed on the surface of the SiO_x anode during prelithiation (**Figure 1**a). As a result, significant improvement in both ICE and cycling stability has been achieved. We believe that the proposed mechanism provides a new perspective on achieving high-capacity Si-based anodes.

2. Results and Discussion

2.1. Screening Molecular Structure for LAC

Theoretically, the reduction potential of the arene molecule should be higher than 0 V versus Li/Li^+ to form LAC and lower than 0.2 V versus Li/Li^+ to enable lithiation in SiO_{x^*} . In this work,

biphenyl (BP) is chosen as the comparative arene molecule with a redox potential to form Li–Bp complex at ≈0.32 V versus Li/Li⁺, which is too high for chemical lithiation in SiO_x. [27] To enhance its reducing capability, we aim to introduce various electrondonating functional groups (-CH₃, -CH₂CH₃, -CH(CH₃)₂, and -OH) in the para-position of benzene ring to increase the electron density. First, computational simulations were carried out to estimate the LUMO energy of these candidate molecules by density functional theory (DFT, Figure S1, Supporting Information). Surprisingly, the LUMO energy of 4,4'-diisopropyl BP (DIPBP) is even higher than that of BP, suggesting it might be unsuitable for SiO_x. By contrast, lowered LUMO energy values of -0.56, -0.52, and -0.28 eV are measured for 4.4'-dimethyl BP (DMBP), DEBP, and 4,4'-dihydroxyl BP (DHBP), respectively. The cyclic voltammogram (CV) of various BP derivatives (Figure S2, Supporting Information) shows that DIPBP, BP, DMBP, DEBP, and DHBP exhibit redox potential $(E_{1/2})$ of 0.41, 0.32, 0.19, 0.13, and -0.1 V versus Li/Li⁺, respectively,

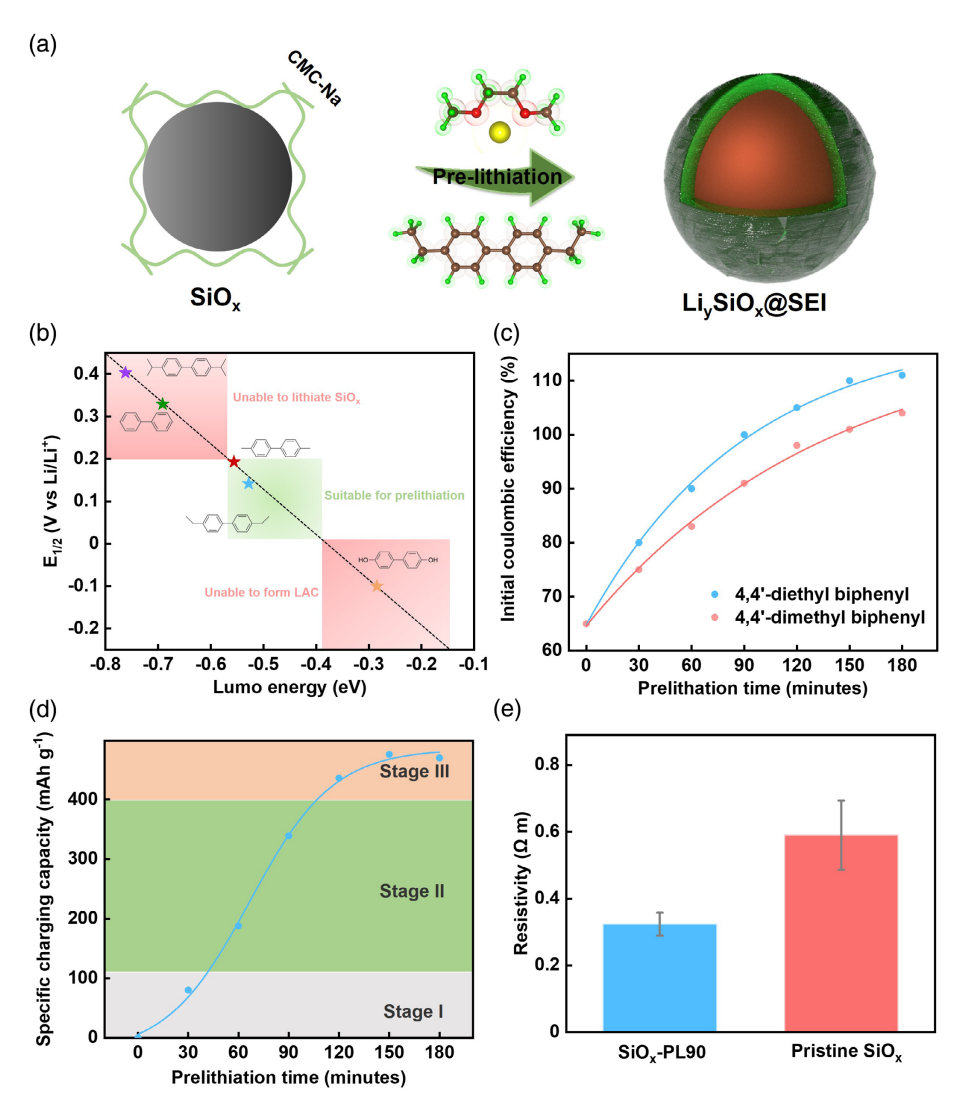


Figure 1. a) Schematic illustration of the chemical prelithiation with SiO_x in the LAC solution; b) correlation between measured redox potential ($E_{1/2}$) of biphenyls with different functional groups and calculated LUMO energy; c) relationship between immersion time and ICE with different BP derivatives; d) relationship between immersion time and specific charging capacity; and e) resistivity of the SiO_x -PL anodes before and after prelithiation.

ADVANCED
ENERGY & SUSTAINABILITY
RESEARCH

www.advenergysustres.com

which highly agree with the estimated LUMO values as the negative shift of the redox potential generally corresponds to an increasing energy level of the frontier molecular orbital. The redox potential of DHBP is lower than 0 V versus Li/Li⁺, inferring that it is stable with Li (as demonstrated in Figure S3, Supporting Information) and cannot form LAC solutions. Moreover, the plot of redox potential of these BP derivatives against their LUMO energy levels shows a good linearity (Figure 1b), suggesting an empirical correlation between the two values can be obtained. In this case, if the redox potential between 0 and 0.2 V versus Li/Li⁺ is desirable for a molecule, its LUMO energy level should fall in the range of -0.41 to -0.57 eV. This finding might be useful for future screening of other potential molecules to prelithiate various electrode materials, depending on the usage scenarios.

As estimated above, DIPBP, BP, DMBP, and DEBP could form blue-green colored LAC solutions (Figure S4, Supporting Information) with metallic Li. From the Fourier transform infrared (FTIR) spectra, the peak emerges at 1074 cm⁻¹ after Li addition corresponds to the asymmetric stretching of C-O-C coordinating Li⁺ in DME, which is indicative of the formation of LAC (Figure S5, Supporting Information). [28] Besides, the UV-vis spectroscopy was also used to evaluate the coordination environment of Li⁺ in LAC (Figure S6, Supporting Information). However, their different reducing capability could result in diverse degrees of prelithiation. As expected, due to their relatively weak reducing capability, LAC based on DIPBP and BP could only enhance the ICE of SiO_x from \approx 65–70% to 71.4% and 77.5% after prelthiation for 2h (Figure S7, Supporting Information). Based on the screening results, DMBP and DEBP are the only two possible candidates for prelithiation application. By contrast, delivering much higher ICE values (over 100%), DMBP and DEBP exhibit much higher lithiation capability (Figure 1c, Figure S8, Supporting Information). In addition, owing to its lower redox potential, DEBP-based LAC achieves higher ICE than DMBP for the same amount of time. Therefore, for efficient prelithiation process, DEBP is finally chosen as the electron-carrying molecule in LAC. As shown in Figure S9, Supporting Information, the SiO_x anode underwent the prelithiation process for 90 min in DEMP (referred as SiO_x-PL90), which shows an ICE as high as 98.6%.

To obtain the kinetic information of the prelithiation process, the amount of active Li within different prelithiated SiO_x anodes was measured by directly charging the half-cells (Figure S10, Supporting Information). As shown in Figure 1d, the formation of active Li first shows low rate due to the side reactions including SEI formation (stage I); then the rate gradually increased (stage II) and became constant (which resembles to galvanostatic charging); eventually as the OCV of SiO_x decreased, the driving force for prelithiation became weaker, hence the slower increase of active Li (stage III). Considering the practical application of this method, the chemical stability of LAC solution and lithiated SiO_x electrodes is critical. After being exposed in dry air (dew point temperature -45 °C), the concentrated LAC solution remained stable (Figure S11, Supporting Information) which does not change the color compared with the as-prepared LAC solutions shown in Figure S4, Supporting Information. Additionally, the prelithiated SiOx anode delivered similar ICE before and after dry air exposure overnight (Figure S12, Supporting Information). Its high chemical stability greatly broadens its potential for industrial use. Interestingly, the areal resistivity of anodes is measured by the four-point probe technique (Figure 1e). It clearly shows that the SiO_x -PL90 anode exhibits a much lower areal resistivity (0.32 Ω m) compared to the pristine electrode (0.58 Ω m), which could be attributed to the exist of active Li (indexed by the Li–Si alloy X-ray diffraction (XRD) peak in Figure S13, Supporting Information). After removing the polyamide protective membrane, the characteristic peaks of $\mathrm{Li}_y\mathrm{SiO}_x$ are found in XRD pattern for prelithiated SiO_x anode (Figure S14, Supporting Information).

2.2. Improved Electrochemical Performance

To date, the impact of prelithiation on the cycling/rate performance of Si-based anodes has drawn very little attention. Herein, the cycling performance of pristine SiO_x and SiO_x-PL90 is compared in Figure 2a. Under 0.2C, the prelithiated SiO_x achieved a specific capacity of 1170 mAh g⁻¹ after 100 cycles, corresponding to a capacity retention of 87.4%; by contrast, the capacity of pristine SiO_x anodes rapidly faded to 897 mAh g^{-1} after 100 cycles, which is only 68.6% of the initial capacity. This result is good in accordance with the electrochemical impedance spectra of different cells after cycling (Figure 2b), where SiO_x results in much higher interfacial resistance compared with SiO_x-PL90. Moreover, the results of rate performance (Figure 2c) show that SiO_x-PL90 possesses superior rate capability over pristine SiO_x. This result can be explained by the higher Li⁺ diffusion coefficients in SiO_x-PL90 than pristine SiO_x at different state of charge (Figure 2d, and S15, Supporting Information).

Then, full cells were assembled by coupling LiCoO₂ (LCO) and LiFePO₄ (LFP) cathode materials with different SiO_x anodes. We applied the prelithiated SiO_x anodes to the full cells. Figure S16, Supporting Information shows that an ICE as high as 90.3% can be achieved by the LCO||SiO_x-PL90 cell, which is much higher than that with pristine SiO_x (65.5%). Accordingly, a much improved energy density (580.5 Wh kg⁻¹, calculated based on the mass of active materials in both electrodes) can be obtained by SiO_x-PL90 compared with that of pristine SiO_x (402.8 Wh kg⁻¹). Moreover, the cycling performance of LCO||SiO_x-PL90 cell is better than LCO||pristine SiO_x cell (Figure 2e). Similarly, the use of prelithiated SiO_x anode, the ICE of LFP-based full cell increased from 70% to 99% and the energy density increased from 313.2 to 443.1 Wh kg⁻¹ (Figure 2f).

2.3. Constructing a Robust SEI ThroughPrelithiation

To investigate the origin of the improved electrochemical performance brought by chemical prelithiation, characterizations of SiO_x anodes before cycling were carried out. Scanning electron microscope (SEM) images of pristine SiO_x (Figure 3a) and SiO_x -PL90 (Figure 3b) confirm that a homogeneous layer is formed on the electrode after chemical prelithiation in LAC solutions. Combining the electrochemical impedance spectra of the SiO_x anodes before and after prelithiation (Figure S17, Supporting Information), this coating layer resembles an

26999412, 2022, 10, Downloaded

doi/10.1002/aesr.202200083 by University Town Of Shenzhen, Wiley Online Library on [24/11/2025]. See the Term

ons) on Wiley Online Library for rules of use; OA articles are governed by the applicable Creative Commons I

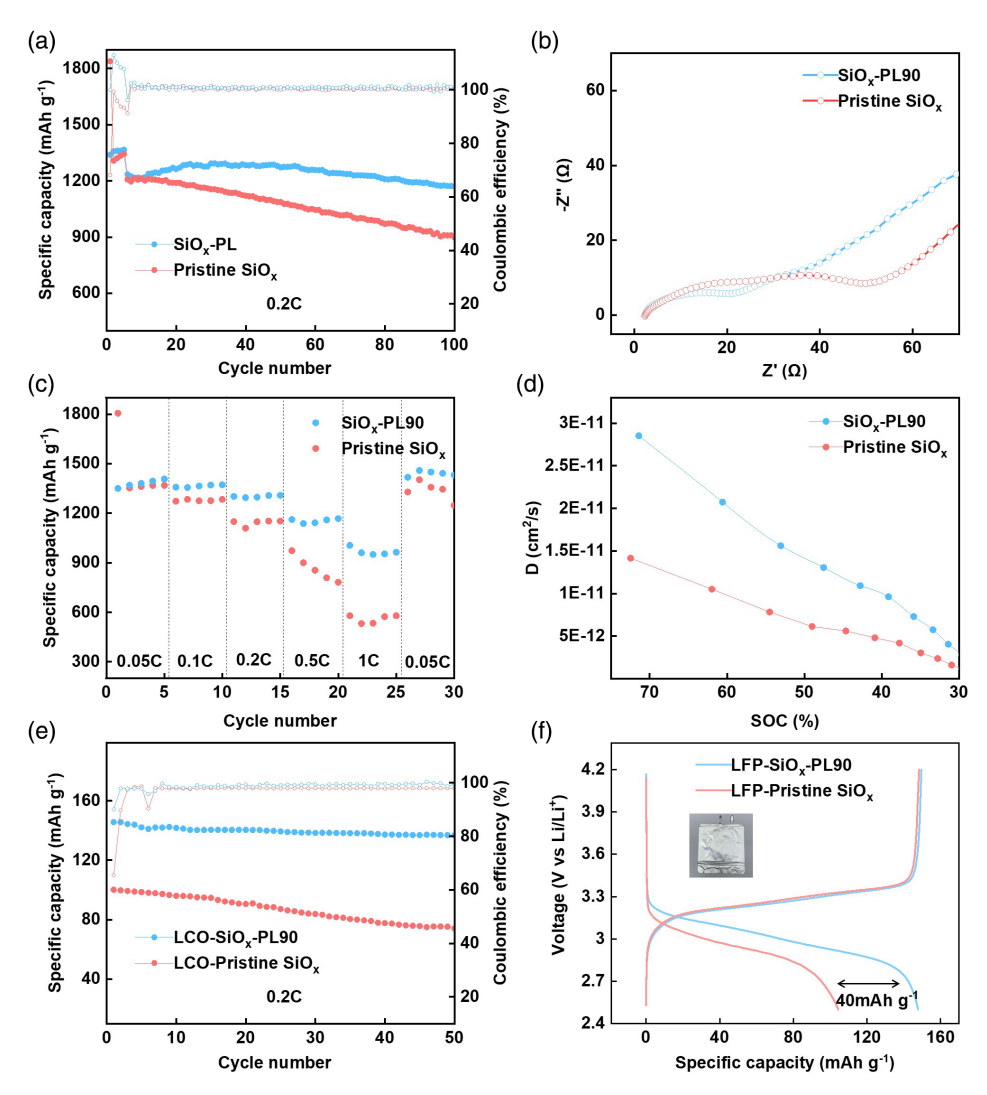


Figure 2. a) Cycling performance of pristine SiO_x and SiO_x -PL90 anodes (the theoretical specific capacity is calculated as $2000 \, \text{mAh g}^{-1}$); b) the electrochemical impedance spectra of pristine SiO_x and SiO_x -PL90 anodes after the fifth cycle; c) rate performance of pristine SiO_x and SiO_x -PL90 anodes; d) measured diffusivities D of Li⁺ versus SOC for GITT with pristine SiO_x and SiO_x -PL90 anodes after five cycles; e) cycling performance of LCO||pristine SiO_x and LCO||SiO_x-PL90 coin-type full cell; and f) voltage profiles of initial discharge–charge cycle of a LFP||pristine SiO_x soft pack full cell and a LFP|| SiO_x -PL90 soft pack full cell.

artificially formed SEI. Additionally, due to the partial Li intercalated into the SiOx, the volume of the active material particles expanded homogeneously throughout the electrode, filling the voids within the pristine electrode. To identify chemical compositions of SEI layer, X-ray photoelectron spectroscopy (XPS) was employed. From Figure 3c and f, the Li 1s spectra show a characteristic peak with high intensity only for the prelithiated SiO_x anodes at 56 eV, which is due to the formation of Li_vSiO_x/Li_vSi and SEI (Figure S18, Supporting Information). The C 1s spectra detect the SEI components after prelithiation. Characteristic peaks of C'-C, C-O, and C=O are identified on the pristine SiO_x anode which is attributable to the presence of binder (CMC) and carbon black (Figure 3d); by contrast, additional characteristic peak of O-CO-O is detected on the prelithiated anode in preformed SEI (Figure 3g), which indicates the presence of lithium carbonate (Li₂CO₃). The Raman spectra of SiO_x-PL90 also confirmed the exist of Li_2CO_3 (Figure S19, Supporting Information). In the Si 2p spectra (Figure 3e, h), the pristine SiO_x exhibits a peak at $103\,\text{eV}$ whereas the Si signal for $\text{SiO}_x\text{-PL90}$ was shielded by the SEI. Combing this result confirms that a dense SEI layer is formed on the surface of SiO_x after prelithiation that shields the Si 2p signal.

Interestingly, as shown in Figure 3i and S20, Supporting Information, this SEI layer cannot be detected on prelithiated SiO_x powders, suggesting the formation of SEI is related to other components in the electrode. As carbon black cannot be oxidized into Li_2CO_3 under such reductive environment, the only possible component leaves to CMC-Na. To confirm this assumption, a CMC-Na film was prelithiated by the LAC. By comparing Figure 3j and Figure S20, Supporting Information, the presence of Li_2CO_3 in the lithiated CMC-Na confirms that the formation of Li_2CO_3 component is attributed to the reaction between CMC-Na

mary.wiley.com/doi/10.1002/aesr.202200083 by University Town Of Shenzhen, Wiley Online Library on [24/11/2025]. See the Terms

on Wiley Online Library for rules of use; OA articles are governed by the applicable Creative Commons

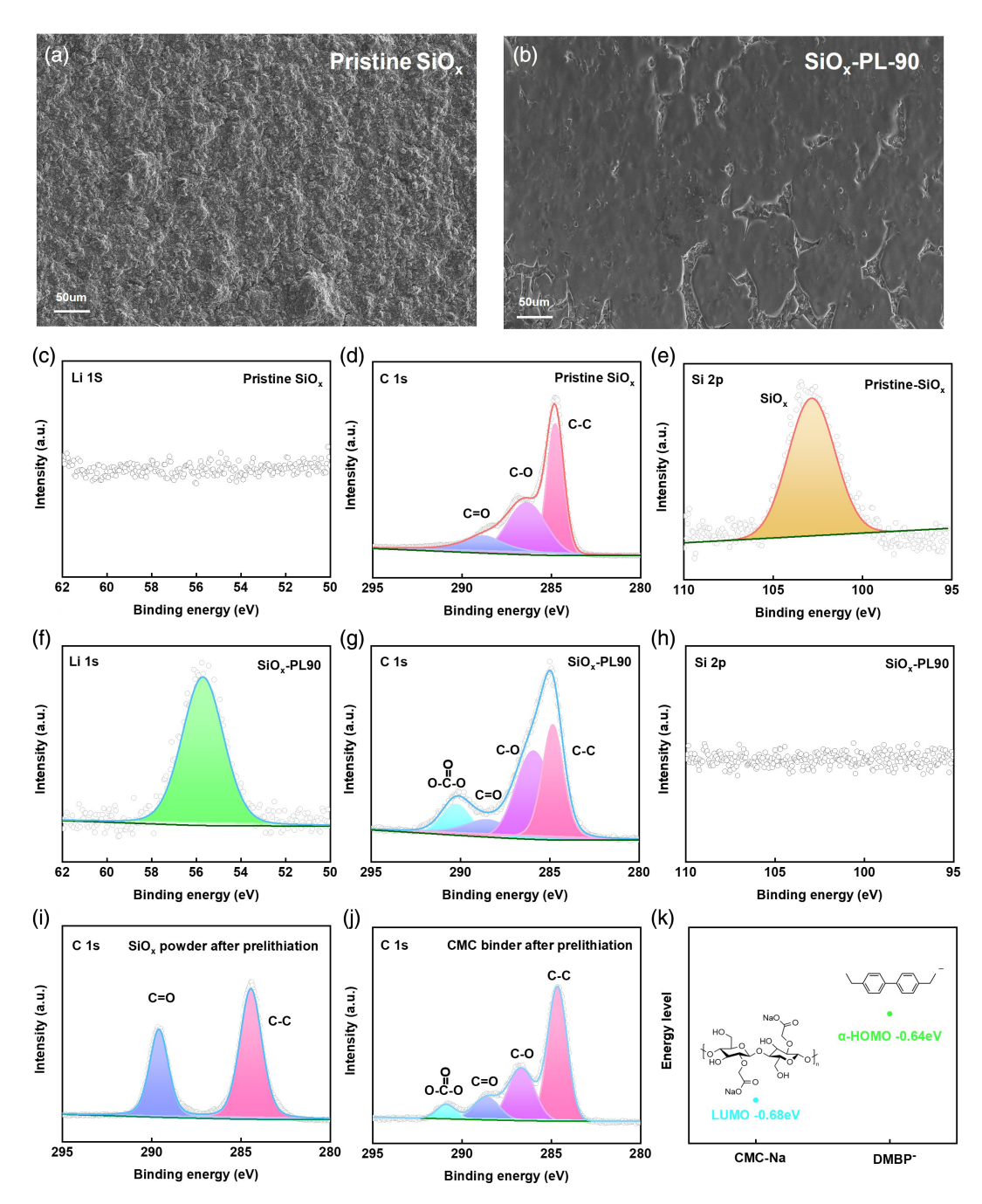


Figure 3. Top-view SEM images of a pristine SiO_x anode a) and SiO_x -PL90 anode b); c) Li 1s XPS spectra of a pristine SiO_x anode; d) C 1s XPS spectra of a pristine SiO_x anode; e) SiO_x -PL90 anode; f) Li 1s XPS spectra of SiO_x -PL90 anode; g) C 1s XPS spectra of SiO_x -PL90 anode; h) SiO_x -PL90 anode; C 1s XPS spectra of SiO_x -PL90 anode; h) Si O_x -PL90 anode; C 1s XPS spectra of O_x -P

and the LAC. [29] The FTIR spectra were also used to evaluate the presence of Li₂CO₃ in the surface of CMC-Na film after prelithiation (Figure S21, Supporting Information). Through DFT simulation, the LUMO energy level of CMC-Na is calculated to be lower than the α -HOMO energy level of DMBP $^-$ in LAC solution, which theoretically supports the feasibility of the reaction between CMC-Na and LAC (Figure 3k). We proposed that the

lithium carboxylate group tends to be attacked by –O–Li group which eventually forms lithium carbonate in LAC solution (Figure S22, Supporting Information).

Thereafter, the pristine SiO_x and SiO_x -PL90 anodes after cycling were also characterized. From Figure S23, Supporting Information, it can be clearly observed that the surface morphology of pristine SiO_x is severely fractured while the active particles

26999412, 2022, 10, Downloaded from https://advanced.onlinelibrary.wiley.com/doi/10.1002/aesr.202200083 by University Town Of Shenzhen, Wiley Online Library on [24/11/2025]. See the Terms

on Wiley Online Library for rules of use; OA articles are governed by the applicable Creative Commons

www.advancedsciencenews.com

www.advenergysustres.com

integrity of prelithiated SiO_x is well preserved. Peeling tests have been also carried out to evaluate the impact of prelithiation process on the adhesive properties of CMC-Na. The adhesion force of prelithiated SiO_x electrode is even greater than pristine SiO_x (Figure 4a). It might because the preformed SEI serves as an elastic anchoring agent between binder and SiO_x particles that will fill up the void (Figure S24, Supporting Information), leading to a better adhesion property. Besides, both electrodes are well preserved after the peeling test (Figure 4b). Therefore, it can be concluded that the adhesive properties of CMC-Na are not compromised by its side reactions with LAC. As shown in Figure 4c, pristine SiO_x shows three characteristic peaks of C-C, C-O, and C=O in the C 1 s spectra. In contrast, the characteristic peaks for C 1s spectra with SiOx-PL90 anodes hardly changed after cycling, suggesting that the preformed SEI remained stable (Figure 4d). In the electrochemical process. CMC-Na did not have side reactions due to the dynamic

constraints. Besides, the content of lithium fluoride (LiF) is higher on the surface of the SiO_x-PL90 anode than that of pristine anode (Figure 4e,f). In this case, the preformed SEI by chemical prelithiation also helps to preserve a LiF-rich SEI, [30] which has been widely reported to be beneficial for the overall performance of Si-based anodes.[31] As illustrated in Figure 4g, it is inferred that compared with SEI layers formed solely during electrochemical processes, the preformed Li₂CO₃ component serves as rigid supporting points, forming an inorganic LiF and Li2CO3 hard-particles plus organic softmixed-compounds robust framework with the CMC-Na binder to suppress the electrode deformation during cycling. The contact between Li₂CO₃ and LiF can promote space charge accumulation along their interfaces, generating a higher ionic carrier concentration. Consequently, a more stable LiF- and Li₂CO₃-rich SEI can be obtained, providing both mechanical strength and improved interfacial Li⁺ transfer.^[32–34]

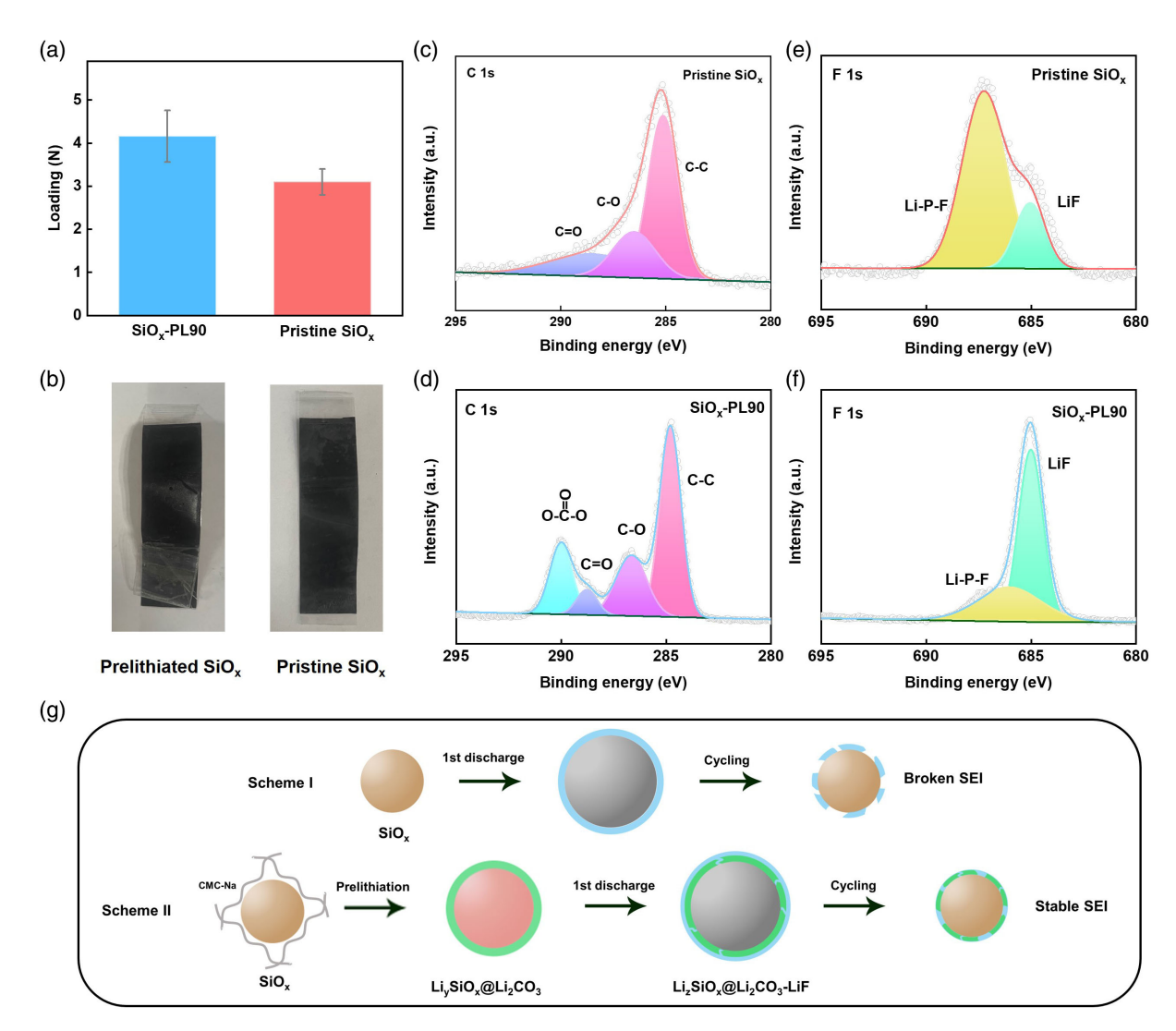


Figure 4. a) Adhesion force of a pristine SiO_x anode and a prelithiated SiO_x anode; b) the optical images of SiO_x electrodes after adhesive force tests; C 1s XPS spectra of a pristine SiO_x anode c) and SiO_x -PL90 anode d) after 100 cycles; F 1s XPS spectra of a pristine SiO_x anode e) and SiO_x -PL90 anode f) after 100 cycles; g) schematic illustration of SEI evolution processes during cycling for pristine SiO_x and prelithiated SiO_x anodes.

and-conditions) on Wiley Online Library for rules of use; OA articles are governed by the applicable Creative Commons

ADVANCED
ENERGY & SUSTAINABILITY
RESEARCH

www.advancedsciencenews.com www.advenergysustres.com

3. Conclusion

In this work, we demonstrated active prelithiation in SiO_x anodes through a stable and scalable chemical solution reaction by introducing various electron-donating groups in the para-position of biphenyl to adjust the reduction potential of LAC solution below 0.2 V. When two ethyl groups are substituted at the para-position, the elevated LUMO levels of 4,4'-diethyl BP decrease the redox potential of LAC solution to 0.13 V, enabling efficient prelithiation. Furthermore, the solution-based prelithiation method facilitates homogeneous reaction between CMC-Na binder and LAC, forming an inorganic LiF and Li₂CO₃ hard-particles plus organic soft-mixed-compounds robust SEI layer on the surface of the SiO_x anode, which remains stable during prolonged cycling. Consequently, improved electrochemical performance can be obtained for prelithiated SiO_x. We believe that the proposed strategy offers great potential of commercial application, which will accelerate the utilization of high-capacity Si-based anodes.

4. Experimental Section

Materials: All biphenyl compounds with different substitution were purchased from Aladdin. Microsized SiO_x was kindly provided by Shenzhen Dajiabang Co. Ltd. and the SiO_x anode electrolyte was obtained from DoDoChem (Suzhou, China).

Preparation of Electrodes: The SiO_x anodes were made by a typical slurry casting method with active materials (SiO_x), conductive carbon (acetylene black), and binder (CMC-Na) at a mass ratio of 5:3:2. The slurry was casted onto a Cu foil current collector and dried at 50 °C for 1 h. The electrodes were further dried in a vacuum at 100 °Covernight and cut into disks with a diameter of 10 mm. The typical mass loading of active materials on each electrode was 0.8 \pm 0.2 mg cm $^{-2}$. The electrolyte was 1.2 M LiPF₆ in 1:1 v/v EC/DEC with 10% FEC and the separator was porous PP films (Celgard 2400). The full cells were designed with an N/P ratio (the practical capacity ratio of the negative electrode to the positive electrode) of 1.2. For cointype full cells, cathodes were fabricated by casting slurry composed of active materials (LiCoO₂), conductive carbon (acetylene black), and binder (PVDF) at a mass ratio of 8:1:1 on an Al foil. For soft pack full cells, the lithium iron phosphate (LiFPO₄) cathode electrodes (Canrd) were dried in vacuum at 80 °C for 2 h before use. Full cells were assembled using same electrolytes and separators as those used in the half-cells.

The Chemical Prelithiation of SiO_x Anodes: The reaction solution was prepared by dissolving lithium metal slice in as-prepared 0.5 M biphenyl compounds with different substitution in DME, and stirring vigorously for 1 h at 44 °C in an Ar-filled glove box. The molar ratio of Li/biphenyl compounds with different substitution was fixed to 4:1 to supply an enough amount of Li. Then, the SiO_x anodes were immersed in the reaction solution for appropriate time and temperature. Next, the SiO_x anodes were rinsed with 1.2 M LiPF₆ in 1:1 v/v EC/DEC with 10% FEC electrolyte to quench further reaction between solution and the SiO_x anodes.

Electrochemical Measurements: The cycling tests were carried out using a Neware battery test system within the voltage range of 2.5–4.2 V (vs Li/Li⁺) for the full cells and 0.01–1 V (vs Li/Li⁺) for the half-cells. The theoretical specific capacity of SiO_x material is defined as 2000 mAh g $^{-1}$. CVs of naphthalene and biphenyl derivatives were recorded at a scan rate of 0.5 mV s $^{-1}$ using electrolytic cell composed of Cu foil (working electrode), Li metal (counter electrode and reference electrode), and 0.5 m LiPF₆ in DME solution with 0.2 m redox-active hydrocarbon as the electrolyte. Prior to the CV measurements, Li metal was passivated by being immersed in 5 m Li-bis(fluorosulfonyl) imide (LiFSI) in DME solution for 1 day in order to prevent direct chemical reduction of the arene molecules at the Li metal surface. The electrochemical impedance spectroscopy (EIS) experiments were performed on an electrochemical workstation (CHI 660 E) in the frequency range of 0.1 Hz to 1 MHz.

Material Characterizations: XRD patterns of the prepared samples were collected by using Bruker D8 ADVANCE diffractometer with a Cu Kα radiation source. Field-emission scanning electron microscopy (ZEISS SUPRA55, Carl Zeiss) was used to observe the top-view morphology of as-prepared samples. The cross-sectional images of the electrodes were obtained using focused ion beam (Scios, FEI) equipment. FTIR spectra were collected on a Nicolet Avatar 360 spectrophotometer (ATR) and the absorption of radiation in the UV-vis region was continuously measured by SHIMADZU UV-2450. The change in chemical state of SiO_x electrodes with prelithiation was analyzed by XPS (ESCALAB 250Xi). The conductivities of electrodes were measured using Keithley 4200-SCS semiconductor characterization system and probe station (PS-100, Lakeshore) at room temperature. Adhesion test of the SiO_x electrodes was conducted on a microcomputer controlled electronic universal testing machine (MDTC-EQ-M12-01). The electrode samples were cropped to strips of $20 \times 80 \, \text{mm}$ and both sides of the samples were attached to 3 M 600 Scotch tapes (20 mm in width) with one end open. The electrodes were peeled off the copper current collector by pulling the Scotch tapes at the angle of 180° at a constant displacement rate of 60 mm min

Theoretical Calculation: All calculations were based on the Gaussian 09 package $^{[35]}$ with the DFT method. We used B3LYP/6-311 + G** theory level to optimize the molecular structure and perform frequency analysis. $^{[36,37]}$ The split-valence-shell Gaussian basis set 6-311 + G** was used for the C, H, O, N, and Li atoms. The calculated energy levels were showed in the GaussView software. The polarized continuum model (PCM) was used to describe the implicit solvent effect on the reduction and oxidation processes of LAC solution. Eps constant of DME (16.9) and epsinf constant of DME (1.9) were used for all PCM calculations.

Supporting Information

Supporting Information is available from the Wiley Online Library or from the author.

Acknowledgements

This work was financially supported by Soft Science Research Project of Guangdong Province (grant no. 2017B030301013).

Conflict of Interest

The authors declare no conflict of interest.

Data Availability Statement

Research data are not shared.

Keywords

initial coulombic efficiencies, lithium-ion batteries, prelithiation, ${\rm SiO}_x$ anodes, solid–electrolyte interphases

Received: May 25, 2022 Revised: July 13, 2022 Published online: August 4, 2022

^[1] B. Kang, G. Ceder, Nature 2009, 458, 190.

^[2] J.-M. Tarascon, M. Armand, Nature 2001, 414, 359.

governed by the applicable Creative Commons

www.advancedsciencenews.com

ADVANCED
ENERGY & SUSTAINABILITY
RESEARCH

www.advenergysustres.com

- [3] Y. H. Wang, S. Zheng, W. M. Yang, R. Y. Zhou, Q. F. He, P. Radjenovic, J. C. Dong, S. Li, J. Zheng, Z. L. Yang, G. Attard, F. Pan, Z. Q. Tian, J. F. Li, *Nature* 2021, 600, 81.
- [4] L. Yang, K. Yang, J. Zheng, K. Xu, K. Amine, F. Pan, Chem. Soc. Rev. 2020, 49, 4667.
- [5] J. Zheng, Y. Ye, F. Pan, Nat. Sci. Rev. 2020, 7, 243.
- [6] T. W. Kwon, J. W. Choi, A. Coskun, Chem. Soc. Rev. 2018, 47, 2145.
- [7] Y. F. Yang, J. L. Yang, F. Pan, Y. Cui, Chinese J. Struct. Chem. 2020, 39, 16.
- [8] H. Xue, Y. Wu, Y. Zou, Y. Shen, G. Liu, Q. Li, D. Yin, L. Wang, J. Ming, Adv. Funct. Mater. 2020, 30, 1910657.
- [9] Z. Liu, Q. Yu, Y. Zhao, R. He, M. Xu, S. Feng, S. Li, L. Zhou, L. Mai, Chem. Soc. Rev. 2019, 48, 285.
- [10] J. Zhong, T. Wang, L. Wang, L. Peng, S. Fu, M. Zhang, J. Cao, X. Xu, J. Liang, H. Fei, X. Duan, B. Lu, Y. Wang, J. Zhu, X. Duan, *Nano-Micro Lett.* 2022, 14, 50.
- [11] F. Holtstiege, P. Bärmann, R. Nölle, M. Winter, T. Placke, *Batteries* **2018**, *4*, 4.
- [12] J. W. Choi, D. Aurbach, Nat. Rev. Mater. 2016, 1, 1.
- [13] C. Sun, X. Zhang, C. Li, K. Wang, X. Sun, Y. Ma, Energy Storage Mater. 2020. 32, 497.
- [14] X. Min, G. Xu, B. Xie, P. Guan, M. Sun, G. Cui, Energy Storage Mater. 2022, 47, 297.
- [15] Q. Sun, J. Li, C. Hao, L. Ci, ACS Appl. Mater. Interfaces 2022, 14, 14284.
- [16] P. Jezowski, O. Crosnier, E. Deunf, P. Poizot, F. Béguin, T. Brousse, Nat. Mater. 2018, 17, 167.
- [17] Y. Abe, M. Tomioka, M. Kabir, S. Kumagai, Sci. Rep. 2022, 12 975
- [18] T. Watanabe, T. Tsuda, N. Ando, S. Nakamura, N. Hayashi, N. Soma, T. Gunji, T. Ohsaka, F. Matsumoto, *Electrochim. Acta* 2019, 324, 134848.
- [19] G. Wang, F. Li, D. Liu, D. Zheng, Y. Luo, D. Qu, T. Ding, D. Qu, ACS Appl. Mater. Interfaces 2019, 11, 8699.
- [20] X. Yue, Y. Yao, J. Zhang, S. Yang, Z. Li, C. Yan, Q. Zhang, Adv. Mater. 2022, 34, 2110337.

- [21] P. Bärmann, M. Mohrhardt, J. E. Frerichs, M. Helling, A. Kolesnikov, S. Klabunde, S. Nowak, M. R. Hansen, M. Winter, T. Placke, Adv. Energy Mater. 2021, 11, 2100925.
- [22] K. Zou, W. Deng, P. Cai, X. Deng, B. Wang, C. Liu, J. Li, H. Hou, G. Zou, X. Ji, Adv. Funct. Mater. 2021, 31, 2005581.
- [23] C. Xin, J. Gao, R. Luo, W. Zhou, Chem. Eur. J. 2022, 414, 202104282.
- [24] Y. Shen, X. Shen, M. Yang, J. Qian, Y. Cao, H. Yang, Y. Luo, X. Ai, Adv. Funct. Mater. 2021, 31, 2101181.
- [25] G. Cong, W. Wang, N. C. Lai, Z. Liang, Y. C. Lu, Nat. Mater. 2019, 18, 390.
- [26] Y. Shen, J. Qian, H. Yang, F. Zhong, X. Ai, Small 2020, 16, 134848.
- [27] J. Jang, I. Kang, J. Choi, H. Jeong, K. W. Yi, J. Hong, M. Lee, Angew. Chem., Int. Ed. 2020, 59, 14473.
- [28] J. Choi, H. Jeong, J. Jang, A. R. Jeon, I. Kang, M. Kwon, J. Hong, M. Lee, J. Am. Chem. Soc. 2021, 143, 9169.
- [29] C. C. Nguyen, T. Yoon, D. M. Seo, P. Guduru, B. L. Lucht, ACS Appl. Mater. Interfaces 2016, 8, 12211.
- [30] T. Liu, L. Lin, X. Bi, L. Tian, K. Yang, J. Liu, M. Li, Z. Chen, J. Lu, K. Amine, K. Xu, F. Pan, Nat. Nanotechnol. 2019, 14, 50.
- [31] J. Chen, X. Fan, Q. Li, H. Yang, M. R. Khoshi, Y. Xu, S. Hwang, L. Chen, X. Ji, C. Yang, H. He, C. Wang, E. Garfunkel, D. Su, O. Borodin, C. Wang, *Nat. Energy* 2020, 5, 386.
- [32] Q. Zhang, J. Pan, P. Lu, Z. Liu, M. W. Verbrugge, B. W. Sheldon, Y. T. Cheng, Y. Qi, X. Xiao, *Nano Lett.* 2016, 16, 2011.
- [33] H. Ye, S. Gui, Z. Wang, J. Chen, Q. Liu, X. Zhang, P. Jia, Y. Tang, T. Yang, C. Du, L. Geng, H. Li, Q. Dai, Y. Tang, L. Zhang, H. Yang, J. Huang, ACS Appl. Mater. Interfaces 2021, 13, 44479.
- [34] N. Qin, L. Jin, Y. Lu, Q. Wu, J. Zheng, C. Zhang, Z. Chen, J. P. Zheng, Adv. Energy Mater. 2022, 12, 2103402.
- [35] M. J. Frisch, G. W. Trucks, H. B. Schlegel, G. E. Scuseria, M. A. Robb, J. R. Cheeseman, G. Scalmani, V. Barone, G. A. Petersson, H. Nakatsuji, X. Li, M. Caricato, A. Marenich, J. Bloino, B. G. Janesko, R. Gomperts, B. Mennucci, H. P. Hratchian, J. V. Ortiz, A. F. Izmaylov, J. L. Sonnenberg, D. Williams-Young, F. Ding, F. Lipparini, F. Egidi, J. Goings, B. Peng, A. Petrone, T. Henderson, D. Ranasinghe, et al. Gaussian 09, Revision A.02, Gaussian, Inc., Wallingford CT 2016
- [36] A. D. Becke, J. Chem. Phys. 1993, 98, 5648.
- [37] C. Lee, W. Yang, R. G. Parr, Phys. Rev. B 1998, 37, 785.